Digital Image Correlation and biaxial test on composite material for anisotropic damage law identification

Jean-Noël Périé, Hugo Leclerc, Stéphane Roux, François Hild

Digital Image Correlation and biaxial test on composite material for anisotropic damage law identification

Jean Noël Périé[a,b,*], Hugo Leclerc[a], Stéphane Roux[a], François Hild[a]

[a] *LMT-Cachan, ENS de Cachan / CNRS UMR 8535 / Université Paris 6 / PRES UniverSud Paris, 61 avenue du Président Wilson, F-94235 Cachan Cedex, France*
[b] *on leave from LGMT (Laboratoire de Génie Mécanique de Toulouse); INSA, UPS, 135 avenue de Rangueil, F-31077 Toulouse, France*

Abstract

The purpose of the work is to extend the use of non conventional tests and full field measurements to the identification of an anisotropic damage law. A Digital Image Correlation technique based on a finite element discretization is used to extract planar displacement fields. The reconditioned Equilibrium Gap Method is then used to retrieve a damage law that accounts for shear softening, a specific form suited to the present application. The identification is shown to reduce to a linear system. The example of a biaxial shear test performed on a cruciform specimen is considered. The approach is first qualified by using displacement fields resulting from a non linear computation with a known damage law. A good agreement is observed between the prescribed and identified laws for distinct parameter settings, even when

*Corresponding author
Email addresses: jean-noel.perie@lmt.ens-cachan.fr (Jean Noël Périé), hugo.leclerc@lmt.ens-cachan.fr (Hugo Leclerc), stephane.roux@lmt.ens-cachan.fr (Stéphane Roux), francois.hild@lmt.ens-cachan.fr (François Hild)

significant noise is added to the displacement fields. The reconstructed displacement fields coincide perfectly with the measurements. The complete scheme is finally tested considering images taken during an experiment performed on a carbon / carbon composite. The identified damage pattern and the corresponding damage values are similar to post-processed maps using classically identified parameters. The reconstructed displacement field accounts for 95 % of the fluctuations observed in the measurements.
Key words: Anisotropic damage, Biaxial test, Composite material, Digital Image Correlation, Equilibrium Gap Method

1. Introduction

Composite materials usually exhibit complex, namely, anisotropic and non linear behaviors. Ceramic Matrix Composites (CMCs) in particular behave in very distinct ways depending on the loading direction wrt. the fiber directions and whether they are subjected to tension or compression. Many models developed in the framework of Continuum Damage Mechanics have been proposed to cope with structural computation needs (Voyiadjis et al., 1998). The damage variables, representing the relative loss of modulus are introduced at distinct scales. Burr et al. (1998), for instance, introduce damage variables at the constituent (micro)scale. Matrix cracking is assumed to be induced by the applied load, namely, damage is driven by the maximum principal strain. Conversely, fiber breakage and interface debonding are related to the fiber directions. Other models proposed for instance by Ladevèze (1995)

or Chaboche and Maire (2002) also account for loading-induced anisotropy but introduce damage variables at the ply (meso)scale. In all cases, the macroscopic behavior of a laminate would result from a homogenization process.

In the specific case of CMCs, a major issue is the lack of available material and stacking sequences. The above mentioned models introduce a large set of parameters related to the state and growth laws. A classical identification procedure thus requires numerous elementary tests. In addition, some parameters, e.g., related to couplings between different damage variables, require complex loading paths and are hardly identified. A validation based on tensile tests is also very restrictive in the sense that it may hide the limits of applicability of the model.

In the past, full field measurements were essentially seen as a complementary means of comparison between experiments and FE simulations (Rastogi, 2000). Modern computation means, multiaxial tests and full field measurements offer the opportunity to test and compare different modelings, but also to identify mechanical parameters (Geers et al., 1999; Avril et al., 2008). One of the main challenges now concerns the design of the experiment. One key issue is to select a geometry and an associated loading leading to relevant levels of damage in a large part of the specimen. Computations are essential at this stage. For natural or synthetic anisotropic and heterogeneous materials, this method offers a unique access to parameters of a constitutive law at a given scale. The wealth of data resulting from kinematic fields of the

tested specimen under non proportional and multi-axial loadings can then be exploited as an entry to inverse methods.

Chalal et al. (2004) proposed to use the framework of the so-called Virtual Fields Method (or VFM (Grédiac, 2004)) to analyze composites. A unidirectional composite loaded in shear was described using a linear increase of damage with strain. An alternative approach, based on a new Digital Image Correlation scheme (Q4-DIC (Besnard et al., 2006)) and on the Equilibrium Gap Method (EGM (Claire et al., 2002, 2004)), the so-called Digital Image Mechanical Identification procedure (DIMI (Roux and Hild, 2008)), allows one to retrieve an isotropic damage law directly from pictures acquired during a single biaxial test performed on a flat cruciform specimen. In the following, it is proposed to extend this work to an anisotropic damage case.

The first part of the paper details the identification procedure. A two-step approach is proposed to go from digital images to an anisotropic damage law. First, the basis of the Q4-DIC technique is briefly introduced and used for retrieving in-plane displacement fields. Then it is shown how the DIMI framework can be generalized when considering an anisotropic damage law. The second part of the paper presents some results of such an approach applied to a biaxial test. A flat cruciform specimen made of $[\pm 45^\circ]$ woven plies is subjected to a shear test. Non linear simulations are first used to check the ability of the method to identify a given damage law. The method is then applied to the corresponding experimental test performed on a 2.5D C/C composite.

2. Digital Image Mechanical Identification

2.1. From images to displacement fields

Among full field measurement techniques (Rastogi, 2000), Digital Image Correlation (DIC) is fast emerging because of its versatility and simplicity of use. It consists in evaluating displacement fields corresponding to a series of (white light) pictures taken at distinct stages of loading. If the natural texture of the material is not sufficient for tracking accurately the displacements, a random speckle is usually sprayed onto the surface. Two gray level images f and g (f stands for the reference picture and g that corresponding to the deformed stage) are related through the local passive advection of the texture by a displacement field $\mathbf{u}$

$$g(\mathbf{x}) = f(\mathbf{x} + \mathbf{u}(\mathbf{x})) \tag{1}$$

The problem consists in *identifying* the best displacement field by minimizing the correlation residual $\int \varphi^2 \mathrm{d}x$ over the whole region of interest, where

$$\varphi(\mathbf{x}) = |f(\mathbf{x} + \mathbf{u}(\mathbf{x})) - g(\mathbf{x})| \tag{2}$$

The minimization of φ is intrinsically a non-linear and ill-posed problem. For these reasons, a weak form is preferred by adopting a general discretization scheme

$$\mathbf{u}(\mathbf{x}) = \sum_{n \in \mathcal{N}} u_n \boldsymbol{\psi}_n(\mathbf{x}) = [\boldsymbol{\psi}(\mathbf{x})]\{\mathbf{u}\} \tag{3}$$

where $\boldsymbol{\psi}_n$ are the vector shape functions, and u_n their associated degrees of freedom. In a matrix-vector format, $[\boldsymbol{\psi}]$ is a row vector containing the values

of the shape functions $\boldsymbol{\psi}_n$, and $\{\mathbf{u}\}$ the column vector of the degrees of freedom. After integration over the domain Ω, the global residual is defined as

$$\Phi = \iint_{\Omega} \left| f(\mathbf{x} + [\boldsymbol{\psi}(\mathbf{x})]\{\mathbf{u}\}) - g(\mathbf{x}) \right|^2 \, \mathrm{d}\mathbf{x} \tag{4}$$

At this level of generality, one may choose to decompose the displacement field on a "mechanically meaningful" basis. When no simple behavior is expected, one may use a "simple" Finite Element kinematic basis (Sun et al., 2005). Here, classical bilinear shape functions associated with quadrilateral 4-node elements (or Q4) (Besnard et al., 2006) are chosen. It is referred to as Q4 Digital Image Correlation (or Q4-DIC). The measured displacement fields are next used as inputs for an independent damage law identification procedure, based on the *same* kinematic description.

2.2. From displacement fields to an anisotropic damage law

2.2.1. Constitutive law and state variables

The material is assumed to be initially homogeneous. Indices $(1, 2)$ refer to the ply coordinate system (i.e., material frame) here coinciding with the fiber directions. With these notations, E_1 and E_2 denote initial Young's moduli (in the fiber directions), G_{12} the initial shear modulus, and ν_{12} one of the Poisson's ratio. The angle between this frame and that of the camera coordinate system (x, y) is denoted by θ (Figure 1). It is first assumed that damage is mainly dictated by the fiber orientation. The damage model considered herein derives from an approach originally introduced by Ladevèze

and Le Dantec (1992). In the following, only one damage variable d_{12} is considered and describes a gradual degradation of the shear modulus. Many [0,90] carbon epoxy woven composites, as a first order approximation, and at a certain scale, behave in a such a way (Gao et al., 1999). A continuum thermodynamics framework is used (Germain et al., 1983). Gibbs' free enthalpy density Φ of woven plies reads

$$\Phi = \frac{1}{2}\left[\frac{\sigma_{11}^2}{E_1} - 2\frac{\nu_{12}}{E_1}\sigma_{11}\sigma_{22} + \frac{\sigma_{22}^2}{E_2} + \frac{\sigma_{12}^2}{G_{12}\left(1-d_{12}\right)}\right] \tag{5}$$

From the state potential Φ, the state laws are derived, and in particular the driving force, $Y_{d_{12}}$ or energy release rate density associated with the damage variable d_{12}

$$Y_{d_{12}} = \frac{\partial \Phi}{\partial d_{12}} = \frac{1}{2}\frac{\sigma_{12}^2}{G_{12}\left(1-d_{12}\right)^2} \tag{6}$$

The driving force $Y_{d_{12}}$ may be expressed in terms of the (indirectly measured) strains

$$Y_{d_{12}} = 2G_{12}\epsilon_{12}^2$$

This force simply depends on elastic parameters and on kinematic quantities. In the sequel, the growth law for d_{12} will be assumed to be controlled solely by its associated thermodynamic force $Y_{d_{12}}$. Let us note that when 3 damage variables are introduced (to account for fiber breakage), other expressions for the driving force of the damage variable d_{12} are proposed, e.g., by Hochard et al. (2007). For the sake of simplicity, the following short-hand notations are used in the sequel $d_{12} = d$ and $Y_{d_{12}} = Y$. An equivalent strain $\epsilon_{eq} =$

$\sqrt{Y/2G_{12}} = |\epsilon_{12}|$ is also defined. This quantity is written in the camera frame (x, y) as

$$\epsilon_{eq} = \left| \frac{1}{2}(\epsilon_{yy} - \epsilon_{xx}) \sin(2\theta) + \epsilon_{xy} \cos(2\theta) \right| \tag{7}$$

Last, one has to identify the parameters of the damage law relating the damage variable d and the maximum over the elapsed time of the equivalent strain ϵ_{eq}.

2.2.2. Identification of a damage law

The Equilibrium Gap Method (EGM) is followed herein (Claire et al., 2002, 2004). It consists in minimizing the force residuals associated with a mismatch of local elastic properties from element to element. It is written in a weak form by using a Finite Element discretization as the minimization of $\|\mathbf{f}_{res}\|^2$

$$\{\mathbf{f}_{res}\} = [\mathbf{K}(\{\mathbf{d}\})]\{\mathbf{u}_{meas}\} - \{\mathbf{f}\} \tag{8}$$

where $\{\mathbf{f}_{res}\}$ is the residual vector associated with measured displacement fields $\{\mathbf{u}_{meas}\}$ and $\{\mathbf{f}\}$ applied nodal forces. Unlike classical FE problems, the aim is to determine the damage fields $\{\mathbf{d}\}$ from known (i.e., measured) displacement fields $\{\mathbf{u}_{meas}\}$ (e.g., by Digital Image Correlation) and the nodal force vector $\{\mathbf{f}\}$ assumed to vanish since only interior nodes are considered. To be consistent with the measured displacements, Q4 elements are used again. The damage variable d is assumed to be element-wise uniform. In the case of anisotropic damage, the elementary stiffness matrix K^{el} is no longer

linear in d (as was the case of an isotropic damage description (Roux and Hild, 2008)) but rather affine

$$K_{ij}^{el} = M_{ij}^{0} - M_{ij}^{1} d \tag{9}$$

where $[\mathbf{M}^0]$ and $[\mathbf{M}^1]$ are matrices dependent upon the initial elastic parameters (of the undamaged element). These elastic constants may also be identified using full field measurements (Lecompte et al., 2007; Roux and Hild, 2008). This point will not be developed herein. To simplify the expressions, an element-wise decomposition of the stiffness matrix is introduced $M_{ij}^{n} = \sum_e M_{ije}^{n}$ (for $n = 0$ or 1), where the sum runs over all elements e. The corresponding contribution of element e to the nodal force at the internal node j is $L_{je}^{n} = \sum_i M_{ije}^{n} u_i$ ($n = 0$ or 1). The problem is expressed by introducing indices for nodes and elements. The idea is to avoid misunderstandings that could be linked to the use of classical FE notations and to explain how the method is implemented. The problem is then equivalent to minimizing the quadratic norm E_g of the "equilibrium gap"

$$E_g = \sum_i \left(\sum_e \left(L_{ie}^{0} - L_{ie}^{1} d_e \right) \right)^2 \tag{10}$$

The solution to such problem would provide a map of shear modulus *contrasts* for each loading step (Claire et al., 2004). The difficulty is to identify a damage growth law, and to link the maps obtained at different loading steps. In the following it is assumed that all the maps result from the *same* damage law. By enforcing that damage grows according to the *same* expression everywhere in the region of interest, the damage law thus minimizes the

equilibrium gap. The regularization of the problem consists in using, at the very beginning of the procedure, a specific decomposition H of the damage law (i.e., a kind of "poor man" Laplace transform)

$$d = H(\widehat{\epsilon_{eq}}, C_k) = \sum_k C_k \varphi_k(\widehat{\epsilon_{eq}}) \tag{11}$$

where $C_k > 0 \quad \forall k$, and with

$$\varphi_k(\widehat{\epsilon_{eq}}) = 1 - \exp\left(-\frac{\widehat{\epsilon_{eq}}}{\epsilon_k}\right) \quad \text{and} \quad \widehat{\epsilon_{eq}} = \max_{0<\tau<t}(\epsilon_{eq}(\tau)) \tag{12}$$

The parameters ϵ_k are preset in order to select the space in which the damage function is searched for. Only ϵ_k values in the range of the experimentally observed equivalent strains are considered. The choice usually made is to set a fixed ratio of 2 between two consecutive values. It corresponds to a good compromise between the conditioning of the system and the number of degrees of freedom used to describe the damage function.

The objective function E_g depends quadratically on the coefficients C_k defining the damage law for the given set of characteristic strains ϵ_k

$$E_g(C_k) = \sum_i \left(\sum_e \left(L^0_{ie} - L^1_{ie} H(\widehat{\epsilon^e_{eq}}, C_k) \right) \right)^2 \tag{13}$$

The above system is not well conditioned because the $[\mathbf{M}^n]$ matrices correspond within the chosen discretization scheme to second order differential operators acting on the displacement field in the continuum limit. Because the displacement field is obtained experimentally, it is inevitably prone to noise and hence the above formulation may suffer from a high sensitivity to this noise, in particular at short wavelengths.

In order to enhance the robustness, it is proposed to introduce the operator $\mathbf{S}$ such that $[\mathbf{S}]\{\mathbf{L}\} = \{\mathbf{u}_{meas}\}$, where $\mathbf{S}$ solves an elastic problem, namely, the medium is assumed to be undamaged. Experimentally determined displacements are applied on the edges as Dirichlet boundary conditions and the body forces $\{\mathbf{L}\}$ are prescribed. The "reconditioned" equilibrium gap objective function $\widetilde{E_g}$ is proposed as given by the following expression

$$\begin{aligned} \widetilde{E_g}(C_k) &= \sum_i \left(\sum_j S_{ij} \sum_e \left(L^0_{je} - L^1_{je} \sum_k C_k \varphi_k(\widehat{\epsilon^e_{eq}}) \right) \right)^2 \\ &= \sum_i \left(u_i - \sum_k C_k \sum_j S_{ij} \sum_e L^1_{ie} \varphi_k(\widehat{\epsilon^e_{eq}}) \right)^2 , \end{aligned} \tag{14}$$

which is read as the quadratic norm of a nodal vector homogeneous to a displacement field. Note that the minimization is to be carried out under the constraint $C_k > 0 \quad \forall k$. In practice, the inverse operator $\mathbf{S}$ is not computed, but rather the "vector" $[\mathbf{S}]\{\mathbf{L}\varphi_k\}$, which is obtained as the solution of an elastic problem for the undamaged solid. In this problem, the material is assumed to be homogeneous, displacements measured on the edges are applied as boundary conditions and body forces are prescribed. A remarkable feature of this procedure is that the identification of the entire (non-linear) damage evolution law is reduced to the resolution of a few linear systems (in practice, only one ore two iterations are needed), with typically few degrees of freedom C_k. This results in particular from the use of a specific decomposition of the damage law [Equation (11)] and from the choice of the norm (10).

3. Validation with synthetic data

The chosen configuration is a biaxial test on a flat [$\pm 45°$] cruciform specimen. The sample is subjected to tension with respect to y and to compression with respect to x (Figure 1). It implies an intense shear strain in the ply coordinate system (Périé et al., 2002). In the following, the focus will be on the identification of the damage part of a model and thus inelastic effects (e.g., related to frictional sliding) are not described. In this first part, the identification procedure is evaluated by using simulated data. The displacement field then results from a non linear FE computation performed with a known damage law. The latter is first used directly and, in a second stage, corrupted with white noise.

The simulations have been performed with an in-house finite element code (Leclerc, 2008). A plane stress state is assumed. The whole cruciform specimen is meshed (Figure 1). The central part of the specimen is uniformly meshed by using 17×17 Q4 elements to be consistent with the measured kinematic field. The displacements computed with this mesh are used as input data for the identification procedure. The arms and the material surrounding the region of interest are meshed by using T3 elements. The angle between the local material coordinate system and the camera coordinate system is set to 45°. The in-plane elastic parameters are such that $E_1 = 35$ GPa, $E_2 = 30$ GPa, $G_{12} = 7$ GPa and $\nu_{12} = 0.1$.

The chosen damage law is decomposed onto the basis described in the previous section. The parameters are $\epsilon_k = 5 \times 10^{-3} \times [1,\ 2,\ 4,\ 8]$ and

$C_k = [0.5,\ 0.3,\ 0.15,\ 0.05]$. The resulting growth law d_{12} *versus* ϵ_k is shown in Figure 2. A non-local approach is used to limit numerical localization effects induced by strain softening. In practice, a mean force $\overline{Y}$ is computed in a given characteristic volume. In some particular cases (e.g., woven composites (Hochard et al., 2007)), the size of this volume may be related to a material characteristic length. In the present case and for the sake of simplicity, $\overline{Y}$ is simply computed over each element. The loading consists in a uniform displacement prescribed at the end of the arms. For both loading directions, normal displacements at the ends of the arms are increased symmetrically step by step, while tangential displacements are forced to 0. The relative displacement between the ends of the two perpendicular directions have the same magnitude but an opposite sign.

Fifteen displacement fields and associated damage fields are computed for equal increments of the relative displacement of the grips. As expected, a moderately heterogeneous damage map is obtained at each loading step. The damage map obtained at the last stage of loading is plotted underneath the deformed mesh (Figure 1). Due to stress (and strain) concentrations, the in-ply multiaxial stresses and the smaller surface of the T3 elements, the mean equivalent strain is higher in the elements that surround the fillet radii than in the rest of the specimen. However, one notes that the associated concentration of damage does not drastically limit the higher damage level that is obtained in the virtual "Region Of Interest (ROI)." With the chosen damage law, a maximum relative displacement of 0.6 % between the ends of

opposite arms leads to a damage level greater than 0.7 in that region.

To assess the quality of the identification, it is first proposed to compare the reconstructed displacement field (using the identified damage field) to the reference data, i.e., the "measured" displacement field. A residual R is defined as the ratio of the standard deviation (denoted by $\chi(.)$) of the difference between the measured and reconstructed displacement fields, normalized by the standard deviation of the measured displacement field

$$R = \frac{\chi(\mathbf{u}_{reconstructed} - \mathbf{u}_{meas})}{\chi(\mathbf{u}_{meas})} \tag{15}$$

The smaller the residual R, the better the result. In the following, this quantity is reported for the last load level. Different trial functions are tested. First, the trial function of the imposed law is used, i.e., $\epsilon_k = 5{\times}10^{-3}{\times}[1\ 2\ 4\ 8]$. The identified parameters are $C_k = [0.49,\ 0.28,\ 0.19,\ 0.03]$. Although the numerical values of the C_k coefficients are different from the imposed ones, ($C_k = [0.5,\ 0.3,\ 0.15,\ 0.05]$), it is seen in Figure 2 that the identified and prescribed damage laws with the chosen equivalent strain are undistinguishable over the range of strains covered by the simulated experiment. This excellent agreement is confirmed by the residual at the last loading step, $R \approx 3.1 \times 10^{-4}$.

Different parameters of the trial functions have then been tested to check the sensitivity of the method to the damage decomposition (Figure 2). For example, identifications achieved with $\epsilon_k = 3 \times 10^{-3} \times [1\ 2\ 4\ 8]$ and $\epsilon_k = 7 \times 10^{-3} \times [1\ 2\ 4\ 8]$ give respectively $C_k = [0.01,\ 0.56,\ 0.19,\ 0.24]$ and

$C_k = [0.88,\ 0,\ 0,\ 0.12]$. In both cases, the agreement is very good. For larger values of ϵ_k the results are less accurate (respectively $R = 3.1 \times 10^{-4}$ at the last loading level and $R = 15.8 \times 10^{-4}$ at the 7^{th} loading level). Parameters ϵ_k that do not follow a geometric sequence have also been tested. As an example, the result for $\epsilon_k = 3 \times 10^{-3} \times [1\ 2\ 3\ 4]$, amounts to $C_k = [0.16,\ 0.25,\ 0.0,\ 0.59]$, and is also shown in Figure 2. Again the result is excellent ($R = 5.2 \times 10^{-4}$ at the last loading level). For all the presented identification cases, a relative difference of less than 0.16 % is measured between computed and identified displacement fields. Moreover, the identified shear damage maps are almost identical to the computed ones.

The noise robustness of the proposed method is now addressed. One adds a white noise with a given standard deviation on the fifteen computed displacement fields. In practice, this standard deviation is set to a fraction of the standard deviation of the first computed displacement field. Two noise levels are considered, namely, 20 and 40 %. This corresponds to realistic levels observed on measured displacement fields (because of the low amplitude of the displacements at the first loading level). To achieve the identification, one first uses only every other displacement field (i.e., 8 steps), and then all levels. For each study, identifications are performed by using 100 random selections of noise.

First, the influence of the number of displacement fields used is illustrated for a given level of noise. With 20 % noise, the identified damage laws based on 100 displacement fields are shown in Figure 3 for 8 levels and Figure 4 for

15 levels. When using all 15 displacement fields, the observed discrepancies decrease slightly in the range of computed damage (up to 0.65). Second, the influence of the noise level is compared when all available data are used. Identified damage laws corresponding to 20 and 40 % are given in Figures 4 and 5. As expected, the discrepancies are larger for higher values of noise. These differences are also revealed by plotting the corresponding relative mean error (Figure 6) and relative standard deviation maps (Figure 7) for both noise levels. However, even for 40 % noise, a reasonable agreement is observed between the mean damage per element and the identified result with uncorrupted data. For the highest values of damage, the relative mean error is less than 5 % and the relative standard deviation less than 3 %. In terms of displacements, the residual R does not exceed 3×10^{-2}, even for 40 % noise. An example of comparison between the last reconstructed and measured displacement fields for such a noise level is shown in Figure 8 ($R = 2.4 \times 10^{-2}$). This analysis indicates that the procedure displays good stability / robustness properties.

In order to quantify the improvements linked to the identified model, one proposes to compare the results to a simple reference computation. One may for instance simulate the displacement fields $\mathbf{u}_{reconstructed}(d = 0)$ for the undamaged solid (homogeneous orthotropic elastic body). On the edges of the ROI, the measured displacements are prescribed as (Dirichlet) boundary conditions. The internal displacements are computed and compared with their measured counterparts (Figure 9). In this case, the displacement dif-

ferences no longer show random patterns (indicating clearly that the modeling should be improved) and the corresponding residual is much higher ($R = 11.4 \times 10^{-2}$). Another measure Q is then proposed

$$Q = \frac{\|\mathbf{u}_{reconstructed} - \mathbf{u}_{meas}\|_2}{\|\mathbf{u}_{reconstructed}(d=0) - \mathbf{u}_{meas}\|_2} \tag{16}$$

Here again, the smaller the quantity Q, the better the result. The error indicator Q is much less than unity ($Q = 20.8 \times 10^{-2}$), indicating a significant improvement.

4. Analysis with experimental data

In this last part, the experiment performed on a so-called 2.5D C/C composite is presented. This woven material has a non-linear behavior when subjected to shear or tension with respect to the fiber direction. The test has been carried out on the multiaxial machine ASTRÉE. A flat cruciform specimen, considered as a [$\pm 45°$] laminate, is subjected to a shear test. Tabs glued on the (100-mm large) arms allow for a transmission of the load to the gauge section (Figure 10). Due to the specimen thickness (i.e., 10 mm), a plane stress state is assumed. This test was designed by means of FE computations to induce a high value of shear damage in the central part of the specimen. Loading and unloading cycles are exploited. The detail of the loading path and of the experimental setup are given in Ref. (Périé et al., 2002). In the present case, 11 pairs of pictures are used. The latter are subsequently used to identify the parameters of the proposed damage law.

Digital images of the surface (1016×1008-pixel resolution, 8-bit depth) are shot at various steps of loading (Figure 10(b and c)). The pictures are analyzed by using the Q4-DIC algorithm. The element size is set to 32 pixels ($\approx$ 3 mm). When using the first image as the reference, the displacement fields results not only from damage but also from inelastic related effects. As it is usually made when a classical identification procedure (based on tensile tests) is followed, one uses the 11 loading / unloading cycles. The hysteretic effects are neglected and the unloading is considered with a frozen state of damage. The first picture is taken at the maximum shear loading and the second one at the following unloaded state (in terms of resultant in each arm (Figure 10(c)). The entries of the EGM correspond to the difference between the displacement fields measured between the reference image and these two pictures. The elastic parameters are identified using a classical procedure based on tensile tests (Périé et al., 2002).

The damage field within the ROI was also computed by using a damage post-processor (Périé et al., 2002). The non linear parameters were identified using the same tensile tests. The woven ply is then modeled as a [0,90] laminate made of unidirectional plies. The shear damage of each ply is reported (Figure 12(a)). One notes a very good agreement between these post-processed damage maps and those determined by following the present procedure (Figure 12(b)). Figure 13 shows a comparison between the measured and reconstructed displacement fields for the last loading step. The corresponding residual is here estimated to be $R = 5 \times 10^{-2}$, higher than

for the artificial cases that were deprived of noise, but still quite low. As proposed earlier, one can also compute the displacement fields corresponding to an undamaged state (Dirichlet boundary conditions applied on a homogeneous and orthotropic elastic body) and compare it to the measurements (Figure 14). The residual then amounts to more than $R = 7.8 \times 10^{-2}$. The improvement linked to the damage modeling is confirmed by the value of Q ($Q = 70.6 \times 10^{-2}$). It is to be underlined that the present approach allows one to identify a damage law with higher levels of damage (Figure 11) then those observed during classical tensile tests (Périé et al., 2002) (typically less than 0.5).

5. Summary and perspectives

A new way of identifying anisotropic damage laws using images taken during a mechanical test was presented. The proposed approach is based on recent developments of two (inverse) methods, namely, finite element Digital Image Correlation and identification based on the equilibrium gap method. The first one allows one to retrieve full-field (FE formatted) displacement fields from images during the loading history. The second one consists in solving an FE problem for which the data are measured displacements and the unknowns the parameters of the chosen trial damage law. The performance of the method was first evaluated using displacement fields resulting from FE non linear computations. A biaxial test on a cruciform specimen made of an orthotropic material was simulated. The results of the procedure, in terms

of identified law and of displacement fields, are excellent, and only weakly sensitive to the basis of chosen trial functions and to noise. The presented results are deemed very encouraging.

The procedure was then applied to analyze a real biaxial test performed on a woven composite. In that case, it is possible to identify in a reliable way the damage pattern quite similar to the one obtained by post-processing the measurements with a classically identified damage model. The damage values are also comparable. The reconstructed displacement field is also very close to the measured one.

This work corresponds to the first step toward the identification of more general constitutive laws when considering anisotropic materials. Future developments will include coupled anisotropic damage and inelasticity, which are important for a full account of the behavior of many composite materials.

Acknowledgements

The support of this research by the "Agence Nationale pour la Recherche" is gratefully acknowledged (VULCOMP project).

References

Avril, S., Bonnet, M., Bretelle, A.-S., Grédiac, M., Hild, F., Ienny, P., Latourte, F., Lemosse, D., Pagano, S., Pagnacco, E., Pierron, F., 2008. Overview of identification methods of mechanical parameters based on full-field measurements. Experimental Mechanics 48 (4) 381-402.

Besnard, G., Hild, F., Roux, S., 2006. "Finite-element" displacement fields analysis from digital images: Application to Portevin-Le Châtelier bands. Experimental Mechanics 46 789-803.

Burr, A., Hild, F., Leckie, F., 1998. On the mechanical behaviour under cyclic loading of ceramic-matrix composites. Computational Mechanics A250 256-263.

Chaboche, J.-L., Maire, J.-F., 2002. A new micromechanics based CDM model and its application to CMC's. Aerospace Science and Technology 6 (2) 131-145.

Chalal, H., Meraghni, F., Pierron, F., Grédiac, M., 2004. Direct identification of the damage behaviour of composite materials using the virtual fields method. Composites Part A: Applied Science and Manufacturing 35 841-848.

Claire, D., Hild, F., Roux, S., 2002, Identification of damage fields using kinematic measurements. Comptes rendus Mecanique 330 729-734.

Claire, D., Hild, F., Roux, S., 2004. A finite element formulation to identify damage fields: The equilibrium gap method. International Journal for Numerical Methods in Engineering 61 (2) 189-208.

Gao, F., Boniface, L., Ogin, S.L., Smith, P.A., Greaves, R.P., 1999. Damage accumulation in woven-fabric CFRP laminates under tensile loading: Part 1. Observations of damage accumulation. Composites Science and Technology 59 (1) 123-136.

Geers, M.G.D., de Borst, R., Peijs, A.A.J.M., 1999. Mixed numerical-experimental identification of nonlocal characteristics of random fibre reinforced composites. Composites Science and Technology 59 (10) 1569-1578.

Germain, P., Nguyen, Q.S., Suquet, P., 1983. Continuum Thermodynamics. ASME Journal of Applied Mechanics 50 1010-1020.

Grédiac, M., 2004. The use of full-field measurement methods in composite material characterization: interest and limitations. Composites Part A: Applied Science and Manufacturing 35 751-761.

Hochard, C., Lahellec, N., Bordreuil, C., 2007. A ply scale non-local fibre rupture criterion for CFRP woven ply laminated structures. Computers and Structures 80 (3) 321-326.

Ladevèze, P., Le Dantec, E., 1992. Damage Modelling of the Elementary Ply for Laminated Composites. Composites Science and Technology 43 257-267.

Ladevèze, P., 1995. A damage computational approach for composites: Basic aspects and micromechanical relations. Computational Mechanics 17 [1-2] 142-150.

Leclerc, H., 2008. Toward higher performance of FEM implementations using lazy evaluation and symbolic programming. In: Proceedings of WCCM-8 and ECCOMAS-8 5^{th} European Congress on Computational Methods in Applied Sciences and Engineering, Venice.

Lecompte, D., Smits, A., Sol, H., Vantomme, J., Van Hemelrijck, D., 2007. Mixed numerical-experimental technique for orthotropic parameter identification using biaxial tensile tests on cruciform specimens. International Journal of Solids and Structures 44 (5) 1643-1656.

Périé, J.-N., Calloch, S., Cluzel, C., Hild, F., 2002. Analysis of a Multiaxial Test on a C/C Composite by Using Digital Image Correlation and a Damage Model. Experimental Mechanics 42 (3) 318-328.

Rastogi, P.K., edt., 2000. Photomechanics. Springer, Berlin, Topics in Applied Physics 77.

Roux, S., Hild, F., 2008. Digital Image Mechanical Identification (DIMI). Experimental Mechanics 48 (4) 495-508.

Sun, Y., Pang, J.H.L., Wong, C.K., Su, F., 2005. Finite element formulation for a digital image correlation method. Applied Optics 44 7357-7363.

Voyiadjis, G. Z., Ju, J.-W., Chaboche, J.-L., edts., 1998. Damage Mechanics in Engineering Materials. Elsevier, Amsterdam, Studies in Applied Mechanics 46.

List of Figures

1 Schematic of the virtual test (a), reference mesh used and damage map obtained at the last load level plotted over the deformed (× 10) mesh (b). 27

2 Prescribed and identified damage laws with different ϵ_k parameters (no data are available in the gray shaded zone). . . 28

3 Prescribed and identified damage laws using 100 × 8 noisy displacement fields with a 20 % noise level. 29

4 Prescribed and identified damage laws using 100 × 15 noisy displacement fields with a 20 % noise level. 30

5 Prescribed and identified damage laws using 100 × 15 noisy displacement fields with a 40 % noise level. 31

6 Relative difference between the identified damage map with uncorrupted displacements and the mean of the identified damage maps using 100 noisy displacement fields. 32

7 Map of relative standard deviation of identified damage fields using 100 noisy displacement fields. 33

8 Comparison between measured and reconstructed displacements, and corresponding differences for the last loading level. 34

9 Comparison for the last loading level between measured and computed displacements resulting from a homogeneous elastic problem with measured Dirichlet boundary conditions. 35

10 Detail of the experimental setup of the shear test (a), ROI and mesh in the initial configuration (b), loading path (c). Note that "compressive" loads are applied along the x direction and "tensile" loads along the y direction. More details can be found in Ref. (Périé et al., 2002) 36

11 Damage law identified using the 11 pairs of images taken during loading/unloadings cycles. 37

12 Comparison of shear damage maps obtained by using a post-processing procedure (Périé et al., 2002) and the technique proposed herein. 38

13 Comparison between measured and reconstructed displacements (expressed in pixels), and corresponding differences for the last loading level. 39

14 Comparison for the last loading level between measured and computed displacements resulting from a homogeneous elastic problem with measured Dirichlet boundary conditions (expressed in pixels). 40

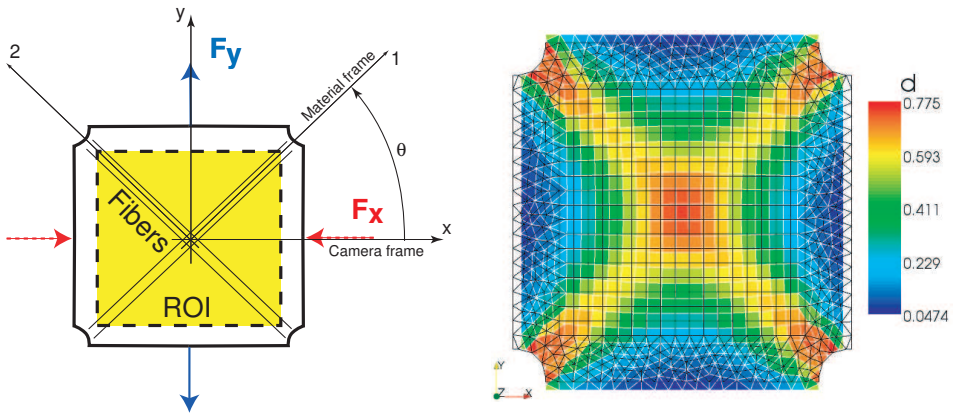

(a) (b)

Figure 1: Schematic of the virtual test (a), reference mesh used and damage map obtained at the last load level plotted over the deformed ($\times$ 10) mesh (b).

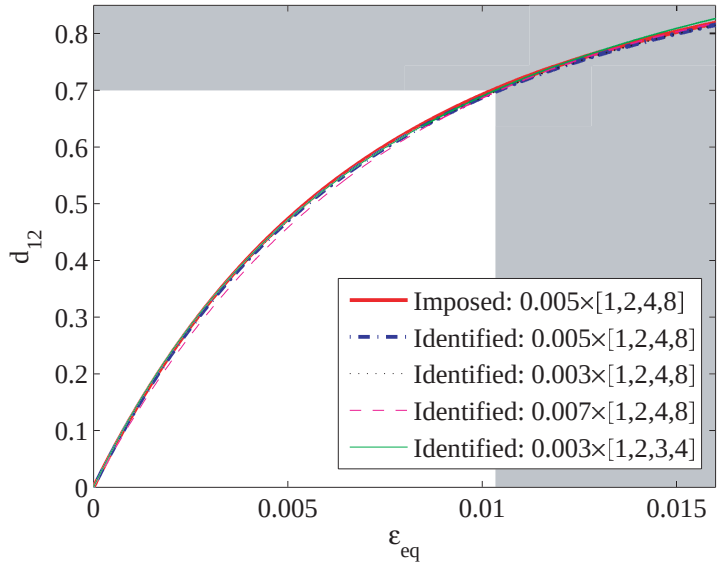

Figure 2: Prescribed and identified damage laws with different ϵ_k parameters (no data are available in the gray shaded zone).

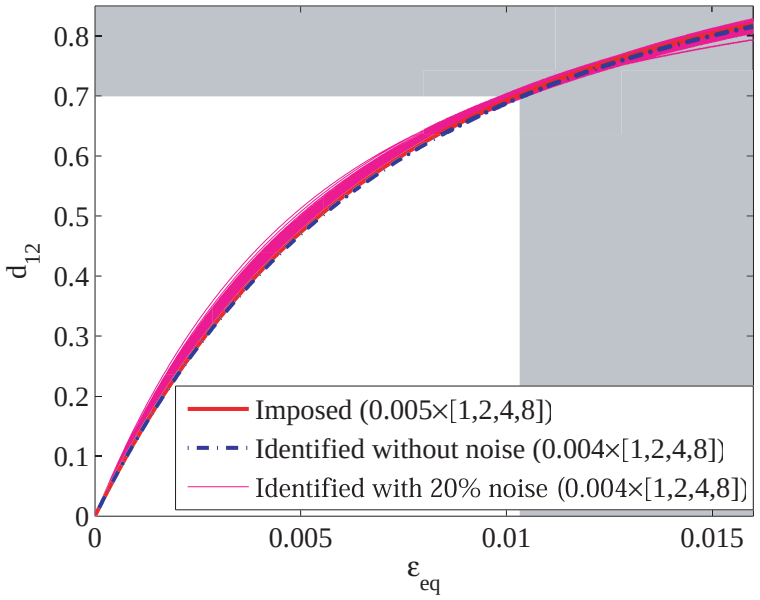

Figure 3: Prescribed and identified damage laws using 100×8 noisy displacement fields with a 20 % noise level.

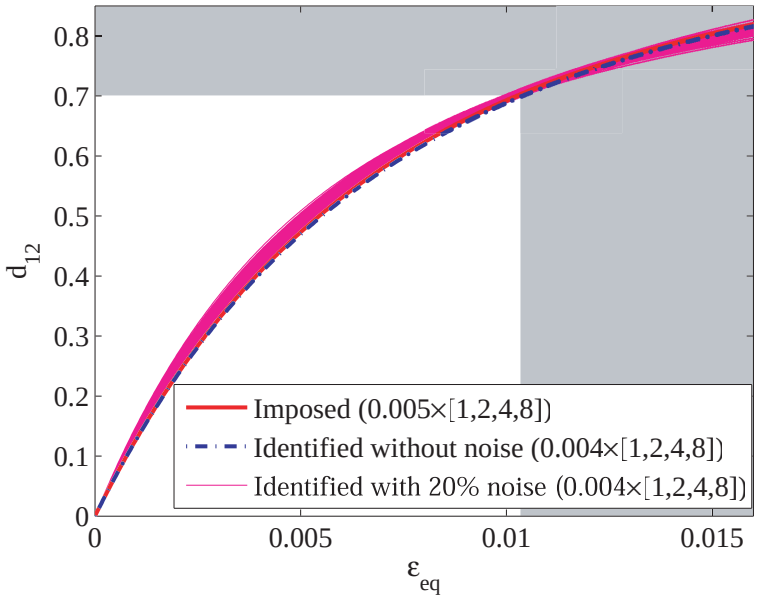

Figure 4: Prescribed and identified damage laws using 100×15 noisy displacement fields with a 20 % noise level.

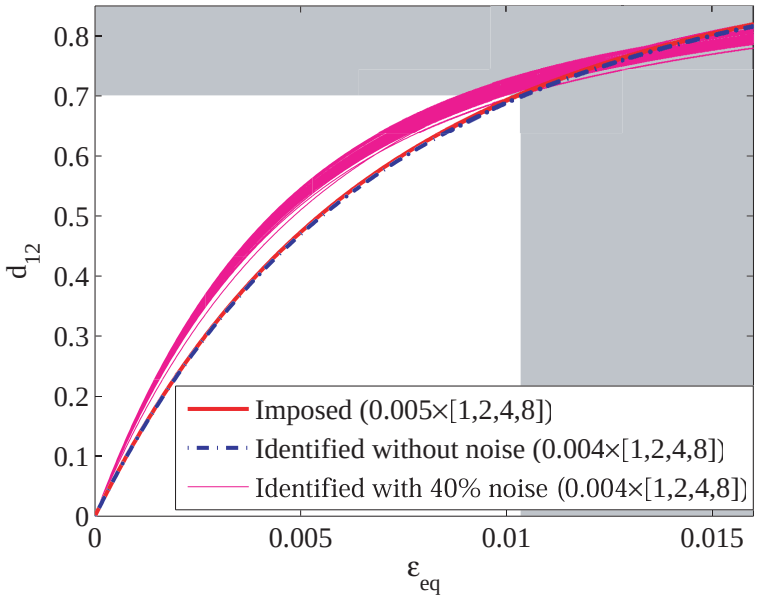

Figure 5: Prescribed and identified damage laws using 100×15 noisy displacement fields with a 40 % noise level.

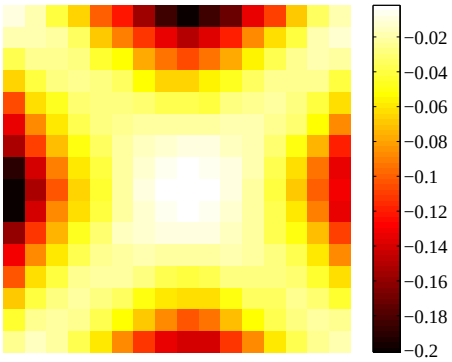

(a) 20 % noise

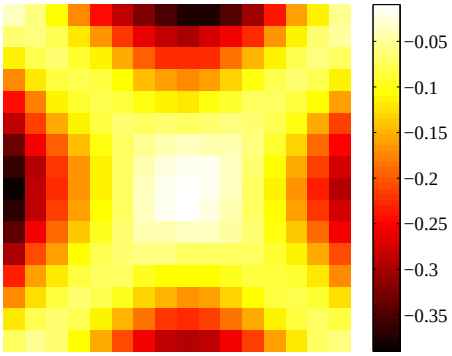

(b) 40 % noise

Figure 6: Relative difference between the identified damage map with uncorrupted displacements and the mean of the identified damage maps using 100 noisy displacement fields.

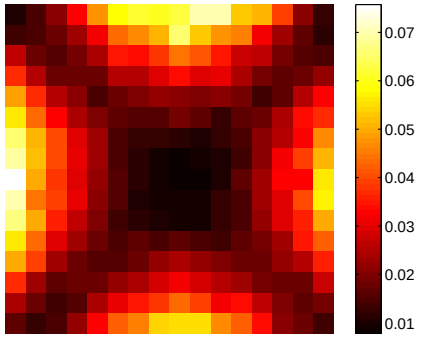

(a) 20 % noise

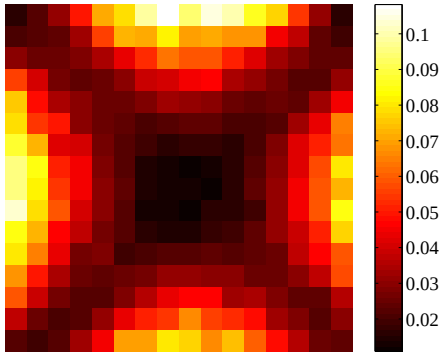

(b) 40 % noise

Figure 7: Map of relative standard deviation of identified damage fields using 100 noisy displacement fields.

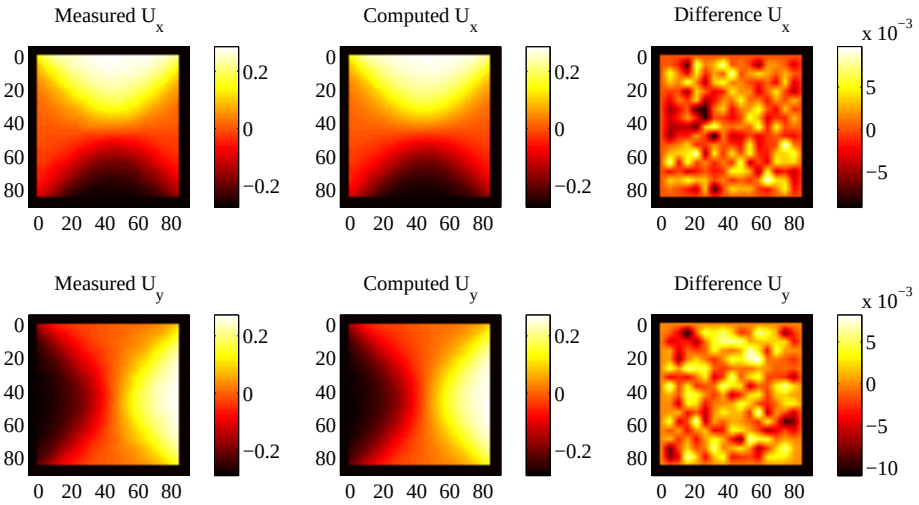

Figure 8: Comparison between measured and reconstructed displacements, and corresponding differences for the last loading level.

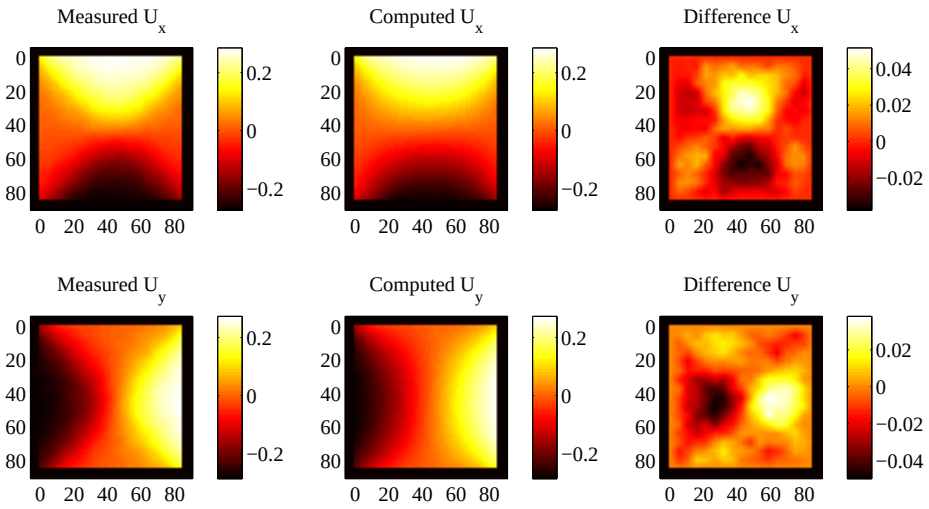

Figure 9: Comparison for the last loading level between measured and computed displacements resulting from a homogeneous elastic problem with measured Dirichlet boundary conditions.

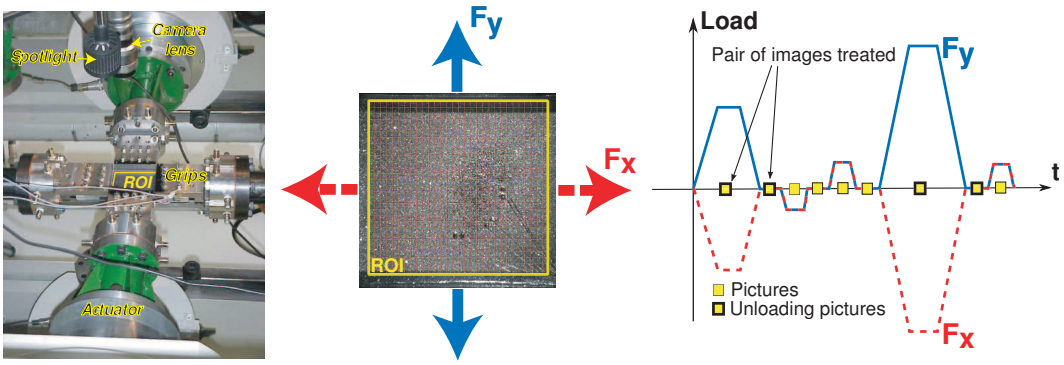

(a) (b) (c)

Figure 10: Detail of the experimental setup of the shear test (a), ROI and mesh in the initial configuration (b), loading path (c). Note that "compressive" loads are applied along the x direction and "tensile" loads along the y direction. More details can be found in Ref. (Périé et al., 2002)

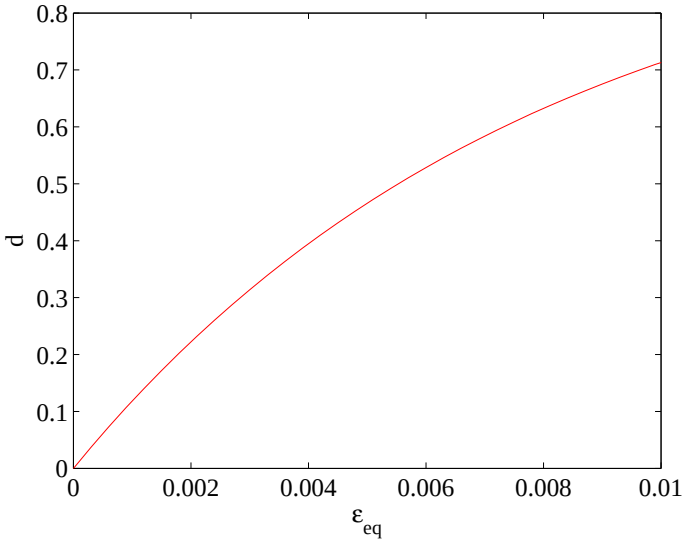

Figure 11: Damage law identified using the 11 pairs of images taken during loading/unloadings cycles.

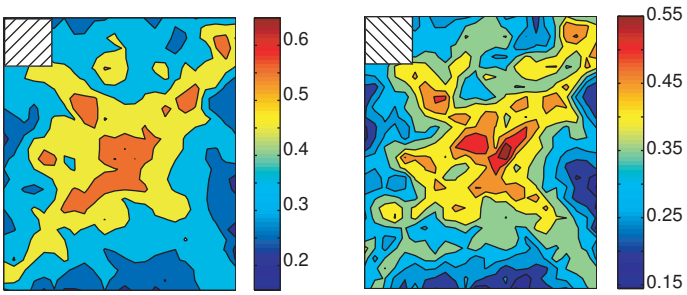

(a) Post-processed in both plies (after (Périé et al., 2002)).

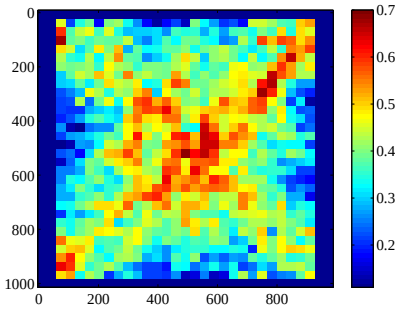

(b) Identified with the present technique.

Figure 12: Comparison of shear damage maps obtained by using a post-processing procedure (Périé et al., 2002) and the technique proposed herein.

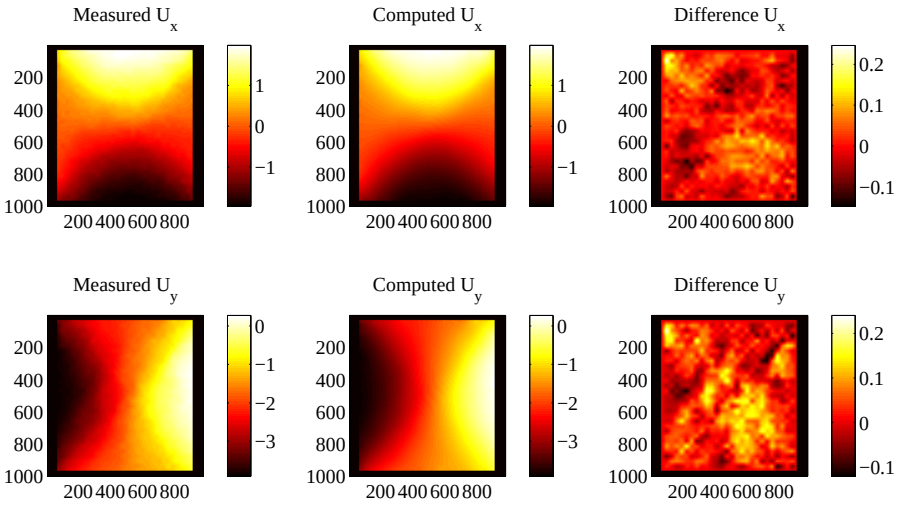

Figure 13: Comparison between measured and reconstructed displacements (expressed in pixels), and corresponding differences for the last loading level.

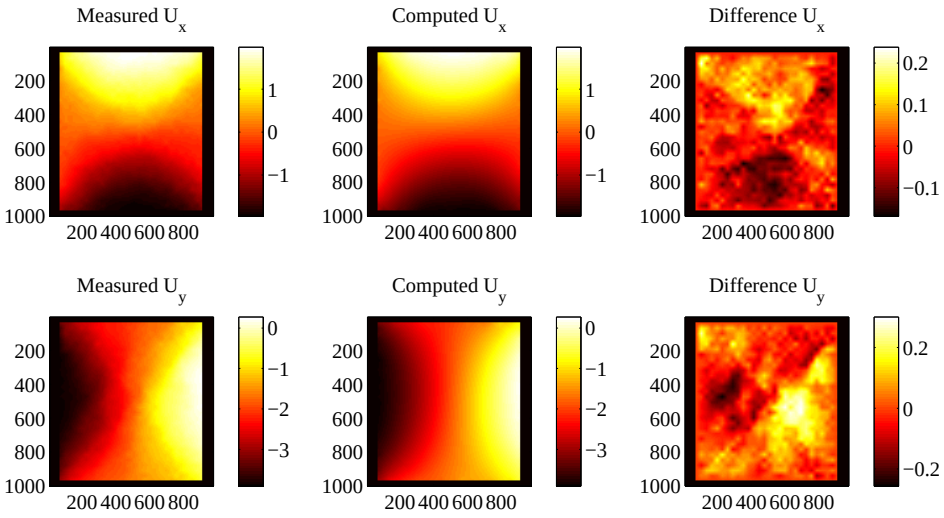

Figure 14: Comparison for the last loading level between measured and computed displacements resulting from a homogeneous elastic problem with measured Dirichlet boundary conditions (expressed in pixels).